The Astronomical Journal, 164:11 (10pp), 2022 July https://doi.org/10.3847/1538-3881/ac6f07

Probing TYC 3315-1807-1, An sdB+dM Binary Displaying Strong Period Variation and Reflection Effect

Shanti Priya Devarapalli[1], Rukmini Jagirdar[1], Vinay Kumar Gundeboina[1], Vineet S. Thomas[2], and Srinivasa Rao Mynampati[3]
[1] Department of Astronomy, Osmania University, Hyderabad, Telangana- 500007, India; astroshanti@osmania.ac.in
[2] The University of Akron, Akron, OH-44304, USA
[3] Formerly from Indian Institute of Astrophysics, Koramangala, Bengaluru, Karnataka, 560034, India
Received 2021 March 4; revised 2022 April 14; accepted 2022 May 4; published 2022 June 15

Abstract

Subdwarf (sdB) stars include core helium-burning stars with a very thin hydrogen envelope that lies at the blue end of the horizontal branch (or extreme horizontal branch). Among them, short-period sdB binaries especially with cool companions are significant to test and constrain binary evolution. We discuss one such sdB+dM type binary, TYC 3315-1807-1 (V1), which was first reported by Kawka. Results of the photometric analysis on Transiting Exoplanet Survey Satellite data are being reported. Light variation in the light curve suggests that the system displays a large reflection effect with no eclipses. Spectroscopic observations of the object were also carried out to probe into the nature of secondary companion as well as to understand the post-common-envelope evolution of such objects. The variability in Balmer, He, and Na line profiles as a function of phase, probably caused by observed reflection effect was identified and studied. Period variation study of the object was done using times of minima obtained from the literature and the $O-C$ plot was produced, which points to a decrease in the period ($dp/dt = -1.36315 \times 10^{-7}$ day yr^{-1}), and the possible scenario of evolution is discussed. From the evolutionary models, we constrain the possible mass of the sdB to be 0.274 $M_{\odot}$ and that of the secondary is 0.113 $M_{\odot}$, and we conclude that V1 may evolve directly as a helium-core white dwarf.

Unified Astronomy Thesaurus concepts: Binary stars (154)

1. Introduction

Subdwarf B (sdB) stars include core helium-burning stars with a very thin hydrogen envelope ($M_{\rm H} < 0.02\ M_{\odot}$, Saffer et al. 1994; Heber 2016) that lie at the blue end of the horizontal branch (or Extreme Horizontal Branch EHB) and some have evolved beyond that stage. Models (Dorman et al. 1993; Han et al. 2003; Heber 2009) predict that mass is most likely to be close to $0.47M_{\odot}$ but binary evolution could produce masses as low as 0.38 or as high as $0.8M_{\odot}$. A significant fraction of these systems are observed in close binary systems (e.g., Maxted et al. 2001; Morales-Rueda et al. 2003; Vučković et al. 2007), which provide ideal conditions for their formation. In close binaries, the onset of the common envelope (CE) phase and subsequent Roche lobe overflow (RLOF) contribute to the ejection of the hydrogen envelope and drive the star toward EHB. The CE phase plays a crucial role in binary evolution, particularly in the formation of short-period systems containing evolved objects, which are known as post-common-envelope binaries (PCEBs). Among PCEBs systems which do not have enough mass to ignite He in their core are known as post-red-giant-branch (RGB) stars. These post-RGBs are known to show low masses with a range of 0.2–0.45 $M_{\odot}$ (Nie et al. 2012).

Han et al. (2002, 2003) proposed three different formation mechanisms for EHB stars through binary interaction: (a) involving CE evolution; (b) episodes of RLOF; or (c) the merger of two helium white dwarfs. All these mechanisms are important as about more than 50% of the close binary population are short-period PCEBs (Maxted et al. 2001; Napiwotzki et al. 2004). Among PCEBs, HW Virginis (HW Vir) is a class of binaries with a hot subdwarf primary and an M-dwarf companion. These are at a crucial phase of stellar evolution and thus act as laboratories to study the nature and formation mechanism of sdBs, which are poorly understood. Many observational studies have been carried out on short-period sdB binaries along with long period sdB binaries. However, there is a gap in the current understanding between theory and observations due to the lack of sufficient observational data for HW Vir type systems leading to accurate determination of their absolute parameters like mass, radius, $T_{\rm eff}$, and physical parameters like period variations, presence of third bodies, phase-dependent spectral line variations, etc. This raises the necessity to carry out further detailed observations of a wide range of sdB binaries to understand their contribution to the formation models/theories.

In this paper, we present inputs on the binary nature of an sdB binary based on low-resolution spectroscopy and the Transiting Exoplanet Survey Satellite (TESS) photometric light curve solutions. The object TYC 3315-1807-1 (R.A.: $03^{\rm h}\,21^{\rm m}\,39\overset{\rm s}{.}629$, decl.: $+47°27'18\overset{''}{.}797$) was shortlisted from the MUCHFUSS catalog (Geier et al. 2011a) of hot subdwarfs and was selected due to its short period and its observability with available facilities. Other common names in literature for this binary are Cl Melotte 20 488, GALEX J032139.8+4727, 2MASS J03213962+4727187, etc. Preliminary results were presented by Kawka et al. (2010) who have reported that TYC 3315-1807-1 (hereafter referred to as V1) is an sdB+dM binary and have determined its period to be 0.26584 ± 0.00004 day. The above-mentioned sdB+dM class of systems are generally referred to as PCEBs of HW Vir class, among which a large

fraction of binaries are noneclipsing and show their binarity only through the reflection effect or radial velocity variations. Variable V1 falls into this category of noneclipsing HW Vir systems. A detailed study of the same is discussed further.

2. Data Collection and Reduction

2.1. Photometry

The data used to carry out photometric analysis was taken from the TESS database and the period of observations lie between 2019 November 3 and 27. The observations from TESS fall in the bandpass 6000–10000 Å, following traditional Cousins *I* band centered at 7865 Å. Known for its photometric precision, the mean error of the TESS photometric data, obtained from the average of errors on individual measurement of observations was about ∼0.003. The data was downloaded from Mikulski Archive for Space Telescopes portal and Simple Aperture Photometry Flux (SAP) was selected over Pre-search Data Conditioning SAP flux in order to avoid trend corrections. A total of 14,846 data points were used for the analysis. Wilson–Devinney (WD) code 2015 (Wilson & Devinney 1971; Wilson & Van Hamme 2013) was used to model the light curves and to derive the basic parameters of V1. The fitting of the light curve was done using *mode 2* of the WD code since neither of the stars is in contact with its Roche lobe. The photometric parameters were set as either fixed or adjustable as per convention generally followed while using WD code (Priya et al. 2011; Schaffenroth et al. 2013). The effective temperature (T_1) of the primary component (sdB star) was adopted from Kawka et al. (2010) and fixed at 27,990 K. The gravity-darkening coefficients g_1, g_2 were fixed to 1 (Von Zeipel 1924) and 0.32 (Lucy 1967), respectively. The bolometric albedo A_1 was set to 1 (Rucinski 1969) and the bolometric limb-darkening coefficients (X_1, X_2, Y_1, Y_2) were fixed after interpolating them using the Van Hamme (1993)'s table with a logarithmic law. The same method was used to derive monochromatic limb-darkening coefficients (x_1, x_2, y_1, y_2), which were taken as adjustable parameters throughout the analysis. Other parameters like inclination (i), mean temperature of secondary star (T_2), the bolometric albedo of secondary (A_2), monochromatic luminosity L_1 of star 1, and dimensionless potentials $\Omega_{1,2}$ of both the components were taken as adjustable parameters.

The mass ratio (q) was constrained using the q-search method to obtain an accurate photometric q. Following the WD routine, the best-fit light curve with minimum residual ($\Sigma = 0.00041$) was obtained for a set of iterations, carried out with different values of i to check for significant changes in q. There was no large variation in q for most of the i values; however, it was impossible to obtain the best fit at values other than $i = 63°$, $q = 0.41$. The light-curve parameters obtained are listed in Table 1 and the best-fit light curve ($R^2 = 99.84\%$) with a corresponding geometric structure of the system at various phases is as shown in Figure 1. The large reflection effect observed in the light curve suggests that the secondary is a cooler component with a temperature of ∼3039 K (spectral type M5V) determined from the iterations. The reflection effect is prominently observed at phase 0.5 of the light curve and the same is also evident with the high value of albedo ($A_2 = 1.9$) of the secondary derived from WD code. Along with the peak-to-peak amplitude of reflection effect ($\Delta I = 0.12$ mag), we approximated the effective temperature of the heated surface (T_h) of the secondary using $T_h = T_1(R_1/\sqrt{(}2)a)^{1/2}$ (Maxted et al. 2002) to be ∼7365.6 K, which shows the strong irradiation effect.

Table 1
Best-fit Photometric Parameters for V1 Derived using WD Method

Element	Solution
Fixed parameters	
P (days)	0.2658
a	1.2049
g_1	1.00
g_2	0.32
[a]T_1(K)	27990
[a] log g	5.34
A_1	1.00
X_1	0.752
X_2	0.656
Y_1	0.244
Y_2	0.103
Adjustable parameters	
$i°$	63.120.62
T_2(K)	3039 ± 29.50
A_2	1.95 ± 0.05
Ω_1	8.8603 ± 0.22
Ω_2	5.0558 ± 0.04
q	0.4126 ± 0.003
L_1	10.9284 ± 0.012
L_2	0.0307
x_1	0.279
x_2	0.670
y_1	0.181
y_2	0.399
Roche radii	
$r_{(h,c)}$ pole	0.1183 ± 0.002, 0.1095 ± 0.001
$r_{(h,c)}$ point	0.1184 ± 0.002, 0.1101 ± 0.001
$r_{(h,c)}$ side	0.1183 ± 0.002, 0.1095 ± 0.001
$r_{(h,c)}$ back	0.1184 ± 0.002, 0.1099 ± 0.001

Notes. (h, c) - (hotter, cooler) components.
[a] T1 and log g adopted from Kawka et al. (2012).

2.2. Spectroscopy

Nine low-resolution spectra were obtained from the 2.3 m Vainu Bappu Telescope (VBT) at the Vainu Bappu Observatory[4] Kavalur, Tamil Nadu, during three nights in 2019 January. The observations were performed using Opto-Mechanics Spectrograph, which uses a Tek 1k × 1k CCD (1024 × 1024 pixels). The spectra were taken in the field centered around 5000 Å with a 600 line mm^{-1} dispersion resulting in a resolution of 2.6 Å pixel^{-1}, such that the Hβ line along with other higher-order Balmer, He, and Na lines can be studied. The above selection was made since Balmer lines are observed to be least affected by reprocessed light from the secondary (Heber & Edelmann 2004). The exposure time for both V1 and the spectrophotometric standard (Feige11) was ∼2400 s. The ONEDSPEC package of IRAF[5] was used to reduce the observed spectral data. The FeNe arc lamp was used

[4] The details of instruments used for spectroscopic observations can be obtained from https://www.iiap.res.in/vbo.htm.
[5] Image Reduction and Analysis Facility.

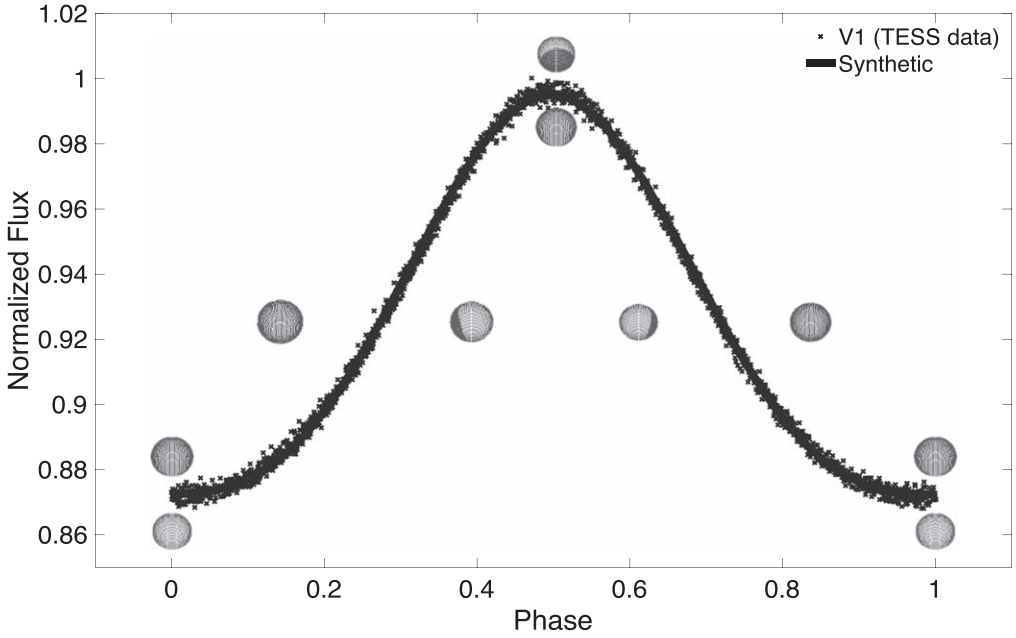

Figure 1. The best-fit light curve of V1 along with star shapes showing reflection effect (dark patches) at various phases.

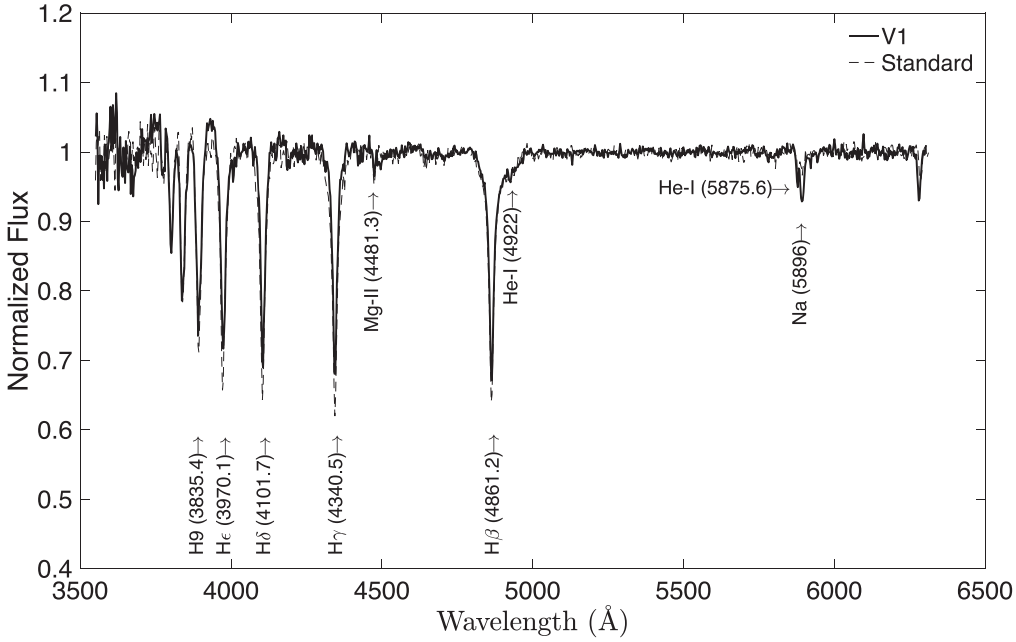

Figure 2. Normalized spectra of V1 overplotted on standard star Fiege11.

for wavelength calibration. The acquired spectra were normalized and equivalent widths (EWs) for the selected lines were measured.

After spectral fitting of the chosen spectral lines with the standard star (Figure 2), the EWs were calculated and tabulated for phases listed in Table 2 (Figure 3). From the phase-dependent spectral line variation (Figure 4), the EWs were observed to be moderately uniform throughout the orbital cycle, except near the upper conjunction, i.e., phase 0.5. It is observed that the Balmer lines appear to be relatively shallower near the upper conjunction. This can be attributed to the excess emission from the heated surface of the cooler component, filling in the absorption line of the sdB. This scenario is similar to that observed for HS 2333+3927 as studied by Shimanskii et al. (2012). We find it likely that the EWs of He and Na lines show variability; however, our observations lack sufficient precision to be certain. As such, this would need higher resolution spectra to determine if the He and Na lines are variable with phase. As the secondary component is M dwarf, which is mostly known to show stellar flares in literature (Chabrier et al. 2007; Yang et al. 2017; Chang et al. 2018), we cannot neglect the effect of flares in them, producing emission and fill-in absorption lines. However, simultaneous high-resolution optical spectra and optical/UV photometry are needed to determine if flares are effecting the line widths. Our present study is an attempt to identify the spectral lines and

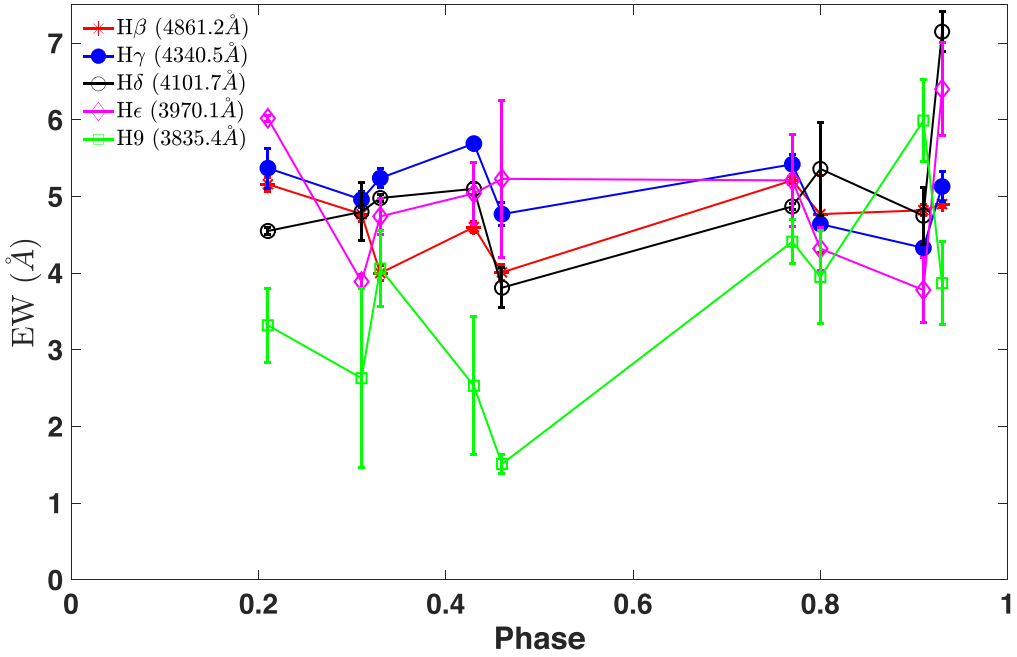

Figure 3. EWs of various Balmer line profiles at various phases.

Table 2
Equivalent Widths of Balmer Lines

Phase	Hβ (4861.2 Å)	Hγ (4340.5 Å)	Hδ (4101.7 Å)	Hϵ (3970.1 Å)	H9 (3835.4 Å)
0.21	5.16 ± 0.09	5.37 ± 0.26	4.55 ± 0.04	6.02 ± 0.04	3.32 ± 0.48
0.31	4.77 ± 0.10	4.96 ± 0.11	4.80 ± 0.38	3.89 ± 0.09	2.63 ± 1.17
0.33	4.00 ± 0.10	5.24 ± 0.12	4.98 ± 0.04	4.74 ± 0.23	4.06 ± 0.50
0.43	4.60 ± 0.07	5.69 ± 0.07	5.10 ± 0.08	5.04 ± 0.41	2.53 ± 0.90
0.46	4.01 ± 0.10	4.77 ± 0.15	3.81 ± 0.26	5.23 ± 1.02	1.51 ± 0.12
0.77	5.21 ± 0.04	5.42 ± 0.13	4.87 ± 0.04	5.21 ± 0.60	4.41 ± 0.29
0.80	4.77 ± 0.50	4.64 ± 0.06	5.36 ± 0.61	4.32 ± 0.28	3.95 ± 0.61
0.91	4.82 ± 0.07	4.33 ± 0.04	4.75 ± 0.37	3.78 ± 0.42	5.99 ± 0.53
0.93	4.90 ± 0.05	5.13 ± 0.19	7.15 ± 0.26	6.40 ± 0.61	3.87 ± 0.54

study presence or absence of variability in their line strengths. Further spectroscopic observations will help us to understand the correlation between the absolute parameters of the DM star and of its radiating surface.

2.3. Period Analysis

As discussed earlier, components in PCEBs mostly tend to be well separated, so period variations that are observed in them cannot be due to mass transfers. However, according to the evolutionary theory, secular period decrease in PCEBs are mostly attributed to angular momentum loss either driven by gravitational radiation (GR), magnetic braking, or due to presence of an unseen substellar or underluminous tertiary companion. The presence of a third body can cause perturbations, in the system causing it to exhibit period variation. To check if V1 shows any variations in the period, we have carried out the $O-C$ (Observed − Calculated times of minima) studies following a series of optimization techniques to determine the best fit. The times of minima (ToM) were collected from the available NSVS, Super WASP, and TESS time-series data. A python code was used to sift through the data to find out local minima in the light curve and a *"scipy"* curve fitting routine was done to extract them (HJD_0). To do this, we first searched for contiguous blocks of data near the minima and then fitted the data with a Gaussian, if there were atleast $\geqslant 7$ points around the minima. Following this, we have obtained 34 ToM (HJD_0) from all the available photometric data. The $O-C$ values are calculated by using the linear ephemeris:

$$\mathrm{MinI} = 2458800.4157788(\mathrm{d}) + 0.265816E. \quad (1)$$

The $O-C$ diagram (Figure 5) shows a decreasing parabolic trend in the period with a dp/dt of $-1.36315(\pm 0.186) \times 10^{-7}$ day yr^{-1}. To know the reason for the period decrease in V1, we checked for the presence of any third light in the system. For this, the light-travel time effect via the presence of a third body was verified by incorporating the l_3 parameter in WD Code but was observed to show a negligible amount of contribution. The period variation plot does not significantly show any sinusoidal signature with the current available data hence, the probability of the presence of a third body in V1 cannot be affirmed. However, the $O-C$ could be a part of a larger sinusoidal variation, which can be confirmed with additional data. Assuming the presence of a third body we tested the $O-C$ with a sinusoidal fit (Figure 5) and the estimated parameters of the third body are listed in Table 3. We also studied period

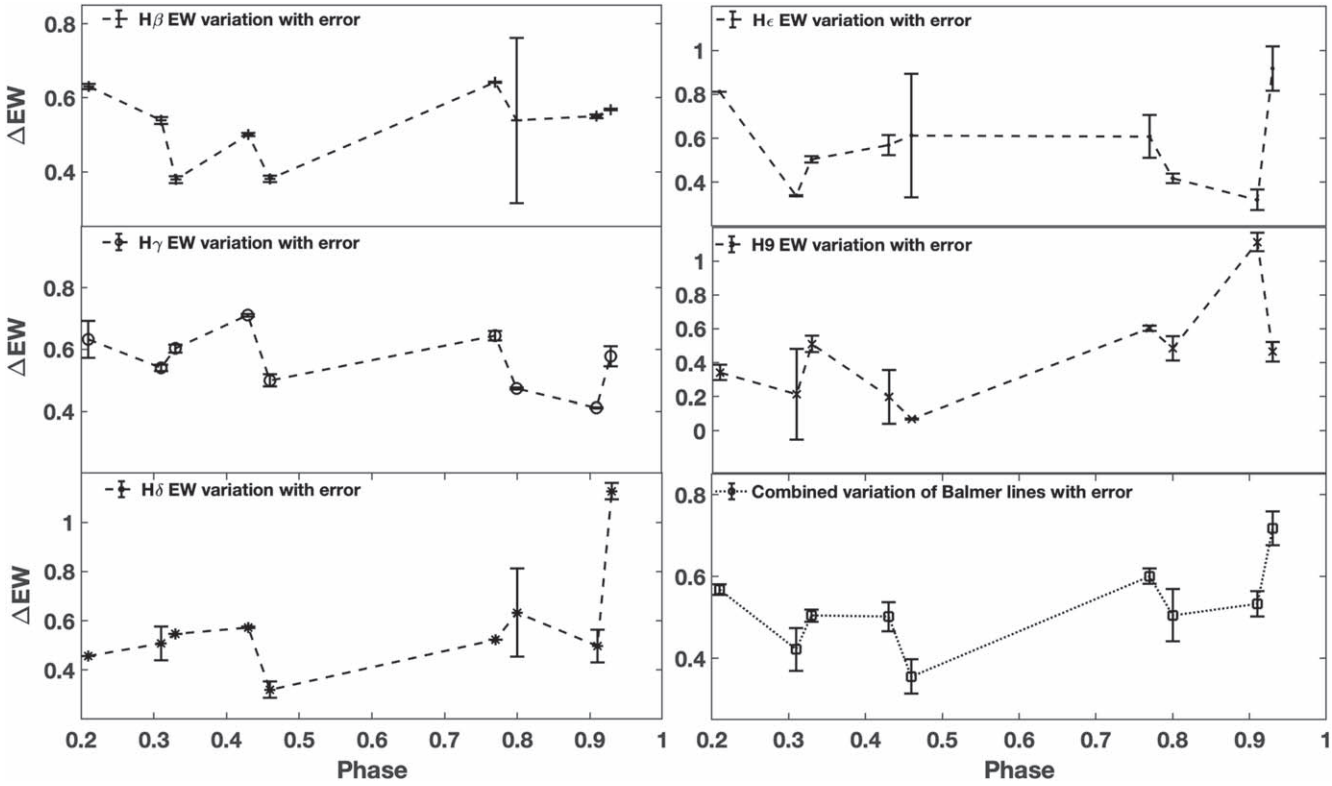

Figure 4. Balmer line profiles showing EW variations.

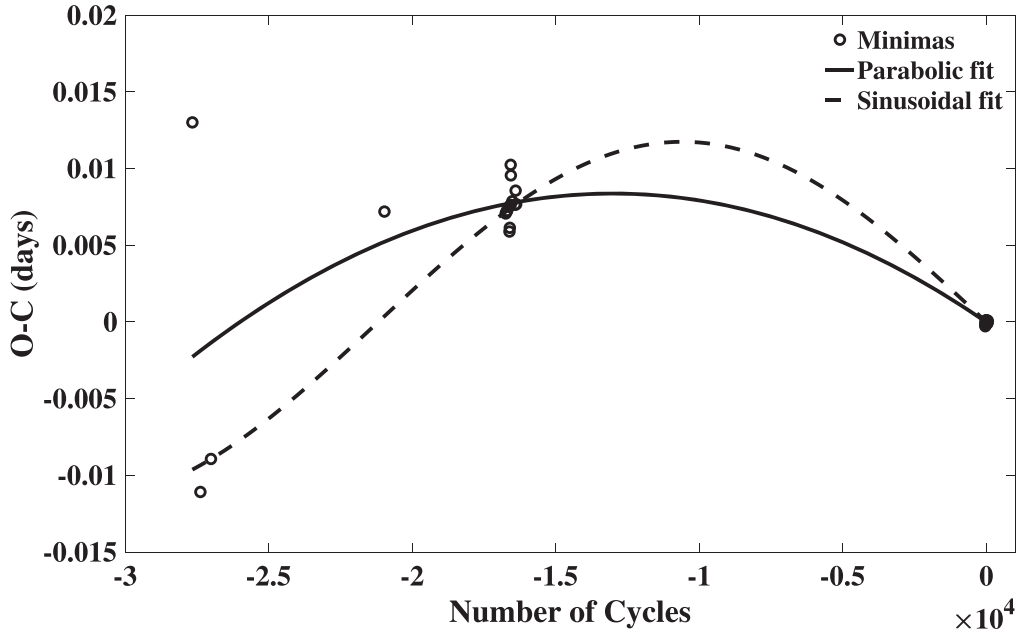

Figure 5. Period variation ($O - C$) for V1 determined from ephemeris and the best fit obtained. The solid line and the dotted line represent the quadratic fit and sinusoidal fit, respectively.

Table 3
Probable Third Body Parameters of V1

Parameter	*Value*	Unit
P_3	30.85 ± 0.748	yr
A_3	0.0059 ± 0.0007	days
$a_{12} \sin i$	1.018 ± 0.157	au
f_m	0.0011 ± 0.00013	$M_\odot$
M_3	0.079 ± 0.011	$M_\odot$

variation in the perspective of gravitational radiation effect along with magnetic braking either of which is generally observed to be dominant in these systems. Based on the relations given by Kraft et al. (1962) and Faulkner (1971), we calculated period change due to GR to be -7.5614×10^{-12} day yr^{-1} and due to magnetic wind braking to be -4.4×10^{-14} day yr^{-1}. Both the values are substantially lower than the observed period variation. Since mass transfer is also ruled out

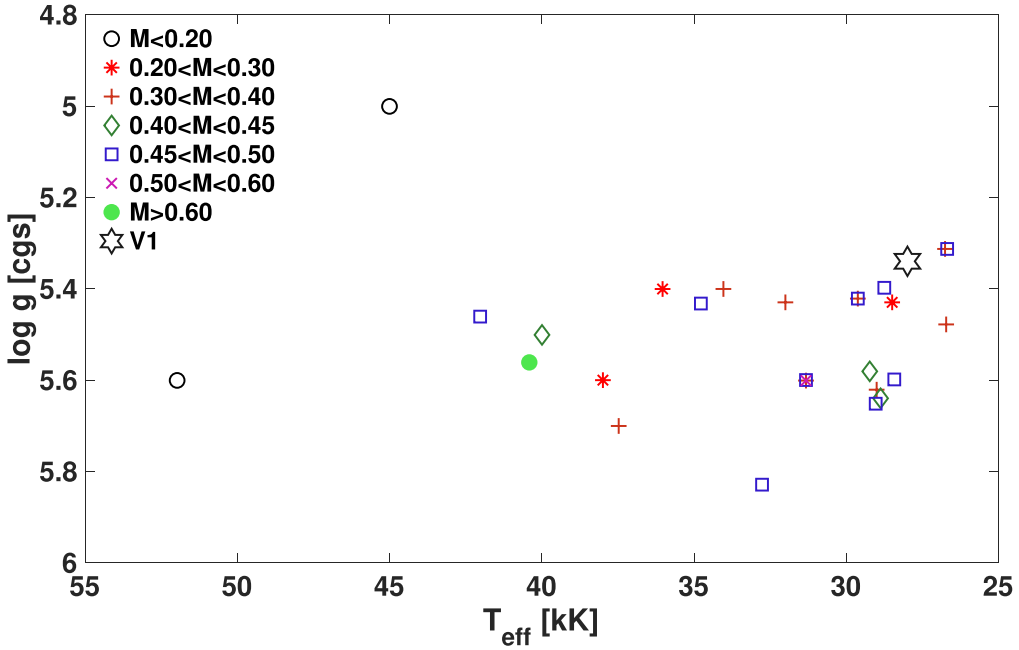

Figure 6. Distribution of sdB's with various masses.

Table 4
Period Variations in HW Vir Systems

S.No	Object	P(days)	dp/dt(day yr^{-1})	$M_3(M_\odot)$	P_3(yr)	References
1	HS 0705+6700	0.0956	⋯	0.037	7.15	Qian et al. (2009)
	⋯	0.0956	⋯	0.029	8.40	Beuermann et al. (2012)
	⋯	0.0956	⋯	0.032	⋯	Qian et al. (2013)
	⋯	0.0956	⋯	0.023	11.70	Bogensberger & Clarke (2017)
	⋯	0.0956	4.20×10^{-9}	0.031	8.73	Pulley et al. (2018)
2	SDSS J08205+0008	0.0962	-1.17×10^{-9}	⋯	⋯	Schaffenroth et al. (2021)
3	NY Vir	0.1010	1.03×10^{-9}	0.003	8.64	Song et al. (2019)
	⋯	⋯	⋯	0.005[a]	24.09	Song et al. (2019)
	⋯	0.1010	9.64×10^{-10}	⋯	⋯	Er et al. (2021)
4	NSVS 14256825	0.1103	3.83×10^{-8}	⋯	⋯	Kilkenny & Koen (2012)
	⋯	0.1103	⋯	0.011	20.00	Beuermann et al. (2012)
	⋯	0.1103	⋯	0.002	3.49	Wittenmyer et al. (2013)
	⋯	0.1103	⋯	0.007[a]	6.86	Wittenmyer et al. (2013)
	⋯	0.1103	⋯	0.014	10.00	Nasiroglu et al. (2017)
	⋯	0.1103	⋯	0.013	8.80	Zhu et al. (2019)
5	HS 2231+2441	0.1105	4.27×10^{-9}	0.013	4.76	Pulley et al. (2018)
6	HW Vir	0.1167	-8.82×10^{-9}	0.018	15.80	Lee et al. (2009)
	⋯	⋯	⋯	0.008[a]	9.10	Lee et al. (2009)
	⋯	0.1167	3.32×10^{-8}	⋯	⋯	Lohr et al. (2014)
7	EC 10246-2707	0.1185	1.23×10^{-9}	⋯	⋯	Pulley et al. (2018)
8	2M 1938+4603	0.1257	-4.49×10^{-8}	⋯	⋯	Barlow et al. (2012)
	⋯	0.1257	⋯	0.002	1.13	Baran et al. (2015)
9	ASAS J102322-3737.0	0.1392	8.45×10^{-8}	⋯	⋯	Lohr et al. (2014)
10	OGLE-GD-ECL-11388	0.1478	-1.1×10^{-8}	0.012	8.91	Hong et al. (2016)
11	AA Dor	0.2615	-6.42×10^{-11}	⋯	⋯	Kilkenny (2011)
12	V1	0.2658	-1.36×10^{-7}	0.079	30.85	present work

Note.
[a] $-M_4$ (Fourth body).

for the system (as it is a detached binary), we suspect that the period variation can be attributed to more than one of the above reasons including the presence of a substellar tertiary component.

3. Discussion and Conclusion

Short-period sdB binaries with low-mass main-sequence companions are important sources in understanding the evolution of sdB stars. The distribution of sdB's with various masses is shown in Figure 6. These binaries can be easily classified by the shape of their light curves, which are dominant with a strong reflection effect due to the large temperature difference between the components. Based on the configuration of the variable in the study, it is suggested that V1 belongs to HW Vir type systems and is a PCEB. In the current study, we present photometric and spectroscopic analysis that show V1 to

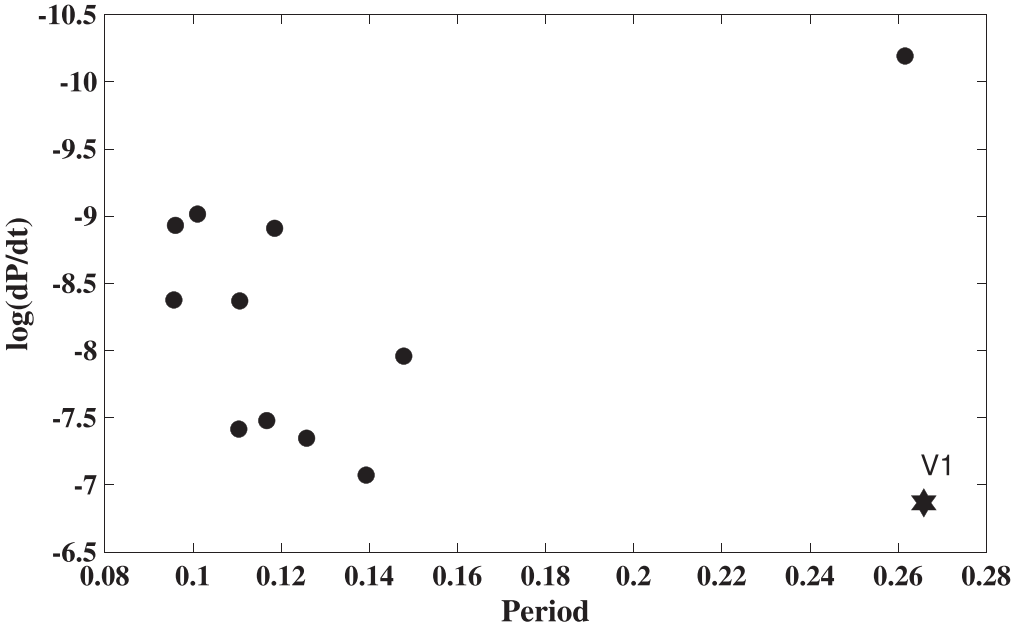

Figure 7. Correlation between period and period variation of HW Vir type systems listed in Table 4.

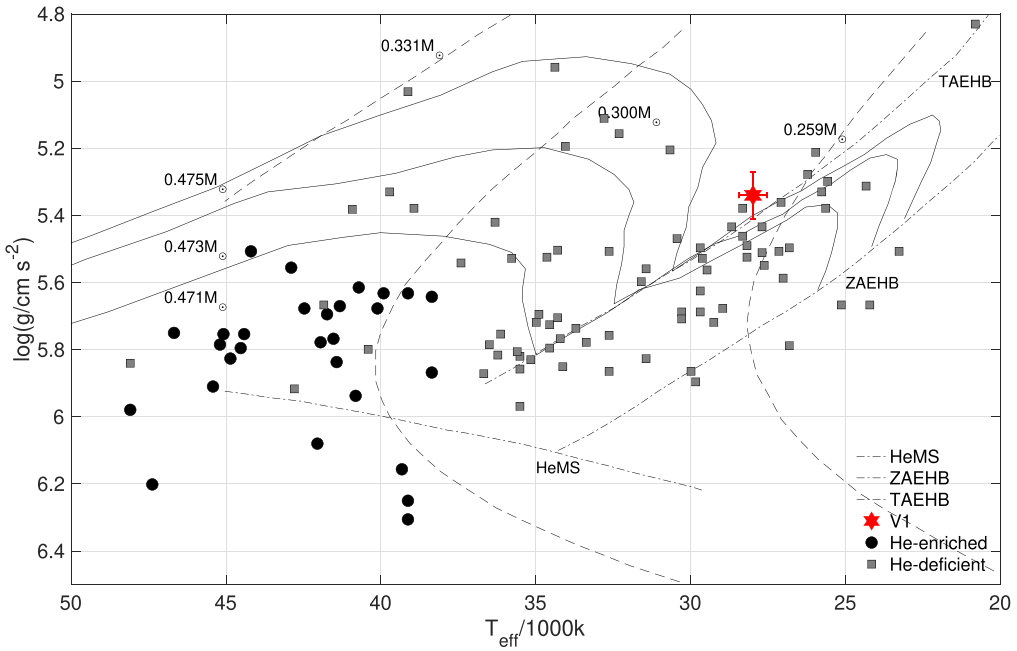

Figure 8. The position of V1 in ($T_{\rm eff}$, log g) diagram is adapted from Heber et al. (2004) compared to other sdB+dM binaries listed in Table 5 and Figure 9 of Heber (2009). The evolutionary tracks for post-EHB evolution is as given by Dorman et al. (1993), and for post-RGB evolution are as given by Driebe et al. (1998).

be a noneclipsing binary with a prominent reflection effect. From spectroscopic analysis, phase-dependent variation in Balmer line profiles are studied and the results are correlated to the reflection effect. The Balmer line profiles measured from low-resolution spectra were matched with synthetic spectra and their equivalent widths were determined. Weak lines of He I 5875 Å, Na 5896 Å, and Mg II 4481 Å could be detected besides strong Balmer lines. Time-resolved high-resolution spectroscopy with a good phase coverage will help us to resolve the contribution to total light by the irradiated surface of cool companion in V1 and also measure $T_{\rm eff}$, log g of subdwarf with high accuracy. The $O-C$ diagram shows a downward parabolic trend, indicating a period decrease at a rate of -1.36315×10^{-7} day yr^{-1}. Since the period decrease cannot be attributed to the mass transfer between the components due to V1's detached configuration, the cause is assumed to be a combined effect of magnetic braking/gravitational radiation or/and the presence of tertiary component. This can be confirmed by longer observational baselines that may support one of the above hypotheses.

To check the nature of period variations in HW Vir systems, data of all HW Vir systems reported with period variation were collected and is as listed in Table 4. Figure 7 shows the correlation between the period and dp/dt of HW Vir systems in literature. It is observed that there is a plausible evidence of period variation observed in most of the HW Vir systems and

Table 5
List of Well-studied HW Vir Type sdB Binaries and V1

S.No	Object	P (days)	$M_1(M_\odot)$	$M_2(M_\odot)$	$R_1(R_\odot)$	$R_2(R_\odot)$	References
sdB Binaries With Calculated Primary Masses							
1	V2008-1753	0.0658	0.47 ± 0.03	0.069 ± 0.005	0.13 ± 0.006	0.08 ± 0.004	Schaffenroth et al. (2015)
2	SDSS J162256.66+473051.1	0.0697	0.39–0.63	0.06–0.07	0.168 ± 0.007	0.085 ± 0.004	Schaffenroth et al. (2014)
3	HS 0705+6700	0.0956	0.48	0.13	0.23	0.186	Drechsel et al. (2001)
4	SDSS J08205+0008	0.0962	0.25–0.47	(0.045–0.068) ± 0.003	⋯	⋯	Geier et al. (2011b)
		0.0962	0.39–0.50	0.06–0.07	0.19 ± 0.008	0.09 ± 0.005	Schaffenroth et al. (2021)
5	PG 1336-018	0.1010	0.5[a]	0.15	0.19 ± 0.01	0.205 ± 0.01	Kilkenny et al. (1998)
		0.1010	(0.38–0.46) ± 0.005	(0.11–0.12) ± 0.001	(0.14–0.15) ± 0.01	(0.15–0.16) ± 0.01	Vučković et al. (2007)
		0.1010	0.45 ± 0.005	⋯	0.15 ± 0.001	⋯	Charpinet et al. (2008)
6	NSVS 14256825	0.1103	0.42 ± 0.07	0.11 ± 0.023	0.188 ± 0.010	0.162 ± 0.008	Almeida et al. (2012)
7	HS 2231+2441	0.1105	0.26 ± 0.010	0.05	0.164 ± 0.005	0.08	Østensen et al. (2008)
		0.1104	0.19 ± 0.15	0.03 ± 0.3	0.143	0.073	Almeida et al. (2014)
		0.1105	(0.19–0.288) ± 0.005	(0.04–0.005) ± 0.0004	(0.144–0.165) ± 0.005	(0.074–0.086) ± 0.004	Almeida et al. (2017)
8	HW VIR	0.1167	0.48 ± 0.09	0.14 ± 0.02	0.176 ± 0.012	0.186 ± 0.011	Wood & Saffer (1999)
		0.1167	0.49 ± 0.013	0.14 ± 0.004	0.183 ± 0.026	0.175 ± 0.026	Lee et al. (2009)
9	EC 10246-2707	0.1185	0.45 ± 0.17	0.12 ± 0.05	0.17 ± 0.02	0.146 ± 0.018	Barlow et al. (2013)
10	2M 1938+4603	0.1257	0.48 ± 0.03	0.12 ± 0.01	⋯	⋯	Østensen et al. (2010)
		0.1257	0.37 ± 0.024	0.10 ± 0.006	⋯	⋯	Barlow et al. (2012)
		0.1257	0.26	0.08	⋯	⋯	Blokesz et al. (2015)
11	ASAS 102322-3737.0	0.1392	0.46 ± 0.051	0.16 ± 0.017	0.179 ± 0.011	0.256 ± 0.015	Schaffenroth et al. (2013)
12	Epic 216747137	0.1610	0.62 ± 0.023	0.11 ± 0.004	0.212 ± 0.005	0.137 ± 0.003	Silvotti et al. (2021)
13	2M 1533+3759	0.1617	0.37 ± 0.055	0.11 ± 0.017	0.166 ± 0.007	0.152 ± 0.005	For et al. (2010)
		0.1617	0.44 ± 0.012	0.12 ± 0.005	0.172 ± 0.002	0.157 ± 0.002	Lee et al. (2017)
14	HS2333+3927	0.1718	0.46 ± 0.08	0.26 ± 0.03	0.16	0.25 ± 0.01	Shimanskii et al. (2012)
15	AA Dor	0.2615	0.33 ± 0.006	0.06 ± 0.002	0.236 ± 0.031	⋯	Rauch (2000)
		0.2615	0.33–0.47	0.064–0.082	0.179–0.200	0.097–0.108	Hilditch et al. (2003)
		⋯	0.46 ± 0.01	0.079 ± 0.002	⋯	⋯	Vučković et al. (2016)
		0.2615	0.46 ± 0.05	0.079 ± 0.009	0.21 ± 0.005	⋯	Baran et al. (2021)
16	EQ Psc	0.8008	0.28 ± 0.10	⋯	0.14 ± 0.02	0.25 ± 0.02	Baran et al. (2019)
17	V1	0.2658	0.274 ± 0.038	0.113 ± 0.016	0.150 ± 0.038	0.139 ± 0.074	Current work
Assumed Canonical Mass							
18	PTF 1 J011339.09+225739.1	0.0933	0.47	0.11 ± 0.003	0.178 ± 0.006	0.16 ± 0.015	Wolz et al. (2018)
19	PTF J072455.75+125300.3	0.0998	0.47	0.15 ± 0.020	0.148 ± 0.007	0.165 ± 0.008	Schindewolf et al. (2015)
20	OGLE-GD-ECL-11388	0.1478	0.47 ± 0.03	0.14 ± 0.02	0.21 ± 0.02	0.19 ± 0.02	Hong et al. (2016)
21	PG 2259+134	0.1634	0.47	0.09 ± 0.008	0.14 ± 0.018	0.09 ± 0.013	Wolz (2018)
22	J192059+372220	0.1689	0.47	0.12 ± 0.007	⋯	⋯	Schaffenroth et al. (2018)
25	PN 2311-18	0.2119	0.47	0.17 ± 0.007	0.17 ± 0.008	0.19 ± 0.009	Wolz (2018)
24	OGLE 416194	0.2666	0.47	0.3 ± 0.04	0.20 ± 0.024	0.28 ± 0.033	Wolz (2018)
25	OGLE 361688	0.2723	0.47	0.15 ± 0.03	0.19 ± 0.04	0.24 ± 0.06	Wolz (2018)
26	OGLE 173411	0.3435	0.47	0.12 ± 0.009	0.22 ± 0.019	0.16 ± 0.015	Wolz (2018)
27	EC 20323-4648	0.4630	0.47	0.17 ± 0.016	0.26 ± 0.028	0.18 ± 0.019	Wolz (2018)

Note.
[a] Assumed mass.

Table 6
Absolute Parameters of V1 in Solar Units

Parameter	$M_{\rm sdB} \sim 0.274 \pm 0.038$
Mass of companion (M_c)	0.113 ± 0.016
Separation (a)	1.268 ± 0.225
Mean radius of sdB (R_h)	0.150 ± 0.038
Mean radius of companion (R_c)	0.139 ± 0.074
Luminosity of sdB (L_h)	12.40 ± 0.760
Luminosity of companion (L_c)	0.002 ± 1.049

the variation is mostly attributed to existence of substellar tertiary objects. Thus, presence of tertiary components in sdB binaries especially in HW Vir systems is not rare and long-term studies on this may lead in understanding their role in formation of such systems.

The evolutionary models in the literature suggest that the mass range of sdB binaries lies between $\sim(0.37–0.48)M_{\odot}$ (Han et al. 2003) with a sharp peak at $0.47M_{\odot}$. Inspite of consistency in literature with defined models in favor of assuming the canonical mass ($0.47M_{\odot}$), it may not be swift to adopt the same due to systematic errors in its determination which in turn depends on model atmosphere. Partial understanding of sdB progenitor evolutionary models, angular momentum coupling within the envelope (Kilkenny et al. 2019), and the need for correction on calculations of opacities direct us toward the need for an improved value of canonical mass. Thus using q, and i obtained from the best-fit WD code and adopting the published amplitude of the radial-velocity curve for the primary star, $K_1 = 60.80 \pm 4.5$ km s^{-1} (Kupfer et al. 2015), we estimated the component masses and radii for V1, using the following mass function relation,

$$\frac{M_1 \times (q \sin i)^3}{(1+q)^2} = \frac{K_1^3 P}{9651904'}, \tag{2}$$

which resulted in sdB mass to be $0.2739 \pm 0.038M_{\odot}$. This mass is too low for a core helium-burning star, indicating that it may be in a critical transition stage of the post-RGB phase of evolution with a thick envelope. Post-RGB phase in sdB's indicates that the star left the RGB early and did not ignite helium in its core. The position of V1 in Figure 8, supports the low mass derived and further it is observed to be lying in the He-deficient region in correlation to the sdBs overplotted for the selected sample substantiating its post-RGB state. Based on the photometric solution obtained and the plausible evolutionary scenario, we suggest that the mass of sdB is $0.27M_{\odot}$ and that of secondary is $0.11M_{\odot}$ (later M-spectral type dwarf). Existence of sdB binaries with low masses as listed in Table 5 indicates that the percentage of such systems in the EHB population is observed to be increasing than before. The absolute parameters derived for V1 for the derived sdB mass are as listed in Table 6.

The obtained low mass of sdB and its unevolved low-mass companion indicates that it has lost its H-envelope on the Hertzsprung gap or has reached RGB early with respect to the mass which is $\leqslant 0.3M_{\odot}$ (Brown et al. 2010). Such objects (post-RGBs) having masses that are too low to sustain helium burning in their cores are believed to form by an extreme mass loss on RGB before they can ignite helium and they tend to directly evolve as white dwarfs with helium core (Driebe et al. 1998). Further, we conclude that the results obtained are only suggestive at this stage, but will be an added inducement to existing understanding on significant empirical mass distribution for sdB stars. Since the theoretical predictions on standard evolutionary scenarios of hot subdwarf populations are challenged by the recent and rather unexpected observational results, studies on such sdB binaries may bridge the gap between the theoretical predictions and observational results. Thus, further work on such sdB binaries should lead in understanding the evolutionary nature of sdBs.

We acknowledge the Director of Indian Institute of Astrophysics, Bengaluru for allocating time for observations at VBT and JCBT. We thank S. Muneer, G. Selva Kumar, P. Anbazhagan, and the observatory staff for helping us during observations. We would like to thank the anonymous referees for their valuable comments which improved the quality of this manuscript. This paper includes data collected by the TESS mission. Funding for the TESS mission is provided by NASA's Science Mission Directorate. Funding for this study was provided in part by a grant from DST-SERB (Project No. EEQ/2017/000411), Government of India.

ORCID iDs

Shanti Priya Devarapalli https://orcid.org/0000-0003-2672-8633
Rukmini Jagirdar https://orcid.org/0000-0002-3007-5164
Vineet S. Thomas https://orcid.org/0000-0001-6447-1176

References

Almeida, L., Damineli, A., Jablonski, F., Rodrigues, C., & Cieslinski, D. 2014, RMxAC, 44, 35
Almeida, L. A., Damineli, A., Rodrigues, C. V., Pereira, M. G., & Jablonski, F. 2017, MNRAS, 472, 3093
Almeida, L. A., Jablonski, F., Tello, J., & Rodrigues, C. V. 2012, MNRAS, 423, 478
Baran, A., Telting, J., Jeffery, C., et al. 2019, MNRAS, 489, 1556
Baran, A., Zola, S., Blokesz, A., Østensen, R., & Silvotti, R. 2015, A&A, 577, A146
Baran, A. S., Østensen, R. H., Heber, U., et al. 2021, MNRAS, 503, 2157
Barlow, B. N., Kilkenny, D., Drechsel, H., et al. 2013, MNRAS, 430, 22
Barlow, B. N., Wade, R. A., & Liss, S. E. 2012, ApJ, 753, 101
Beuermann, K., Breitenstein, P., Debski, B., et al. 2012, A&A, 540, A8
Blokesz, A., Baran, A., & Zola, S. 2015, EPJ Web of Conf., 101, 06010
Bogensberger, D., Clarke, F., & Lynas-Gray, A. E. 2017, OAst, 26, 134
Brown, W. R., Kilic, M., Prieto, C. A., & Kenyon, S. J. 2010, ApJ, 723, 1072
Chabrier, G., Gallardo, J., & Baraffe, I. 2007, A&A, 472, L17
Chang, H.-Y., Lin, C.-L., Ip, W.-H., et al. 2018, ApJ, 867, 78
Charpinet, S., Van Grootel, V., Brassard, P., et al. 2008, in ASP Conf. Ser. 392, Hot Subdwarf Stars and Related Objects (San Francisco, CA: ASP), 285
Dorman, B., Rood, R., & O'Connell, R. 1993, ApJ, 419, 596
Drechsel, H., Heber, U., Napiwotzki, R., et al. 2001, A&A, 379, 893
Driebe, T., Schoenberner, D., Bloecker, T., & Herwig, F. 1998, A&A, 339, 123
Er, H., Özdönmez, A., & Nasiroglu, I. 2021, MNRAS, 507, 809
Faulkner, J. 1971, ApJL, 170, L99
For, B.-Q., Green, E. M., Fontaine, G., & Shaw, S. 2010, Ap&SS, 329, 87
Geier, S., Hirsch, H., Tillich, A., et al. 2011a, A&A, 530, A28
Geier, S., Schaffenroth, V., Drechsel, H., et al. 2011b, ApJL, 731, L22
Han, Z., Podsiadlowski, P., Maxted, P. F., Marsh, T. R., & Ivanova, N. 2002, MNRAS, 336, 449
Han, Z. W., Podsiadlowski, P., Maxted, P. F., & Marsh, T. R. 2003, MNRAS, 341, 669
Heber, U. 2009, ARA&A, 47, 211
Heber, U. 2016, PASP, 128, 082001
Heber, U., Drechsel, H., Østensen, R., et al. 2004, A&A, 420, 251
Heber, U., & Edelmann, H. 2004, Ap&SS, 291, 341
Hilditch, R. W., Kilkenny, D., Lynas-Gray, A. E., & Hill, G. 2003, MNRAS, 344, 644

Hong, K., Lee, J. W., Lee, D. J., et al. 2016, PASP, 129, 014202
Kawka, A., Pigulski, A., O'Toole, S., et al. 2012, in ASP Conf. Ser. 452, Hot Subdwarf Stars and Related Objects (San Francisco, CA: ASP), 121
Kawka, A., Vennes, S., Németh, P., Kraus, M., & Kubát, J. 2010, MNRAS, 408, 992
Kilkenny, D. 2011, MNRAS, 412, 487
Kilkenny, D., & Koen, C. 2012, MNRAS, 421, 3238
Kilkenny, D., O'donoghue, D., Koen, C., Lynas-Gray, A. E., & Van Wyk, F. 1998, MNRAS, 296, 329
Kilkenny, D., Worters, H. L., & Lynas-Gray, A. E. 2019, MNRAS, 485, 4330
Kraft, R. P., Mathews, J., & Greenstein, J. L. 1962, ApJ, 136, 312
Kupfer, T., Geier, S., Heber, U., et al. 2015, A&A, 576, A44
Lee, J. W., Kim, S. L., Kim, C. H., et al. 2009, AJ, 137, 3181
Lee, J. W., Youn, J. H., Hong, K., & Han, W. 2017, ApJ, 839, 39
Lohr, M. E., Norton, A. J., Anderson, D. R., et al. 2014, A&A, 566, A128
Lucy, L. B. 1967, ZA, 65, 89
Maxted, P. F. L., Heber, U., Marsh, T. R., & North, R. C. 2001, MNRAS, 326, 1391
Maxted, P. F. L., Marsh, T. R., Heber, U., et al. 2002, MNRAS, 333, 231
Morales-Rueda, L., Maxted, P. F. L., Marsh, T. R., North, R. C., & Heber, U. 2003, MNRAS, 338, 752
Napiwotzki, R., Karl, C. A., Lisker, T., et al. 2004, Ap&SS, 291, 321
Nasiroglu, I., Goździewski, K., Słowikowska, A., et al. 2017, AJ, 153, 137
Nie, J. D., Wood, P. R., & Nicholls, C. P. 2012, MNRAS, 423, 2764
Østensen, R., Green, E., Bloemen, S., et al. 2010, MNRAS: Letters, 408, L51
Østensen, R., Oreiro, R., Hu, H., Drechsel, H., & Heber, U. 2008, in ASP Conf. Ser. 392, Hot Subdwarf Stars and Related Objects (San Francisco, CA: ASP), 221
Priya, D. S., Sriram, K., & Rao, P. V. 2011, RAA, 11, 175
Pulley, D., Faillace, G., Smith, D., Watkins, A., & Von Harrach, S. 2018, A&A, 611, A48
Qian, S.-B., Shi, G., Zola, S., et al. 2013, MNRAS, 436, 1408
Qian, S.-B., Zhu, L.-Y., Zola, S., et al. 2009, ApJL, 695, L163
Rauch, T. 2000, A&A, 356, 665
Rucinski, S. 1969, AcA, 19, 245
Saffer, R. A., Bergeron, P., Koester, D., & Liebert, J. 1994, ApJ, 432, 351
Schaffenroth, V., Barlow, B. N., Drechsel, H., & Dunlap, B. H. 2015, A&A, 576, A123
Schaffenroth, V., Casewell, S. L., & Schneider, D. 2021, MNRAS, 501, 3847
Schaffenroth, V., Geier, S., Drechsel, H., et al. 2013, A&A, 553, A18
Schaffenroth, V., Geier, S., Heber, U., et al. 2014, A&A, 564, A98
Schaffenroth, V., Geier, S., Heber, U., et al. 2018, A&A, 614, A77
Schindewolf, M., Levitan, D., Heber, U., et al. 2015, A&A, 580, A117
Shimanskii, V., Yakin, D., Borisov, N., & Bikmaev, I. 2012, ARep, 56, 867
Silvotti, R., Schaffenroth, V., Heber, U., et al. 2021, MNRAS, 500, 2461
Song, S., Mai, X., Mutel, R. L., et al. 2019, AJ, 157, 184
Van Hamme, W. 1993, AJ, 106, 2096
Von Zeipel, H. 1924, MNRAS, 84, 665
Vučković, M., Aerts, C., Østensen, R., et al. 2007, A&A, 471, 605
Vučković, M., Østensen, R., Németh, P., Bloemen, S., & Pápics, P. 2016, A&A, 586, A146
Wilson, R. E., & Devinney, E. J. 1971, ApJ, 166, 605
Wilson, R. E., & Van Hamme, W. 2013, ApJ, 780, 151
Wittenmyer, R. A., Horner, J., & Marshall, J. P. 2013, MNRAS, 431, 2150
Wolz, M. 2018, PhD thesis, Friedrich-Alexander-Universitat Erlangen-Nurnberg, https://www.sternwarte.uni-erlangen.de/docs/theses/2018-04_Wolz.pdf
Wolz, M., Kupfer, T., Drechsel, H., et al. 2018, OAst, 27, 80
Wood, J. H., & Saffer, R. 1999, MNRAS, 305, 820
Yang, H., Liu, J., Gao, Q., et al. 2017, ApJ, 849, 36
Zhu, L.-Y., Aian, S.-B., Lajús, E. F., Wang, Z.-H., & Li, L.-J. 2019, RAA, 19, 134